Bias correction and assimilation of microwave radiance measurements over the Antarctic

Craig S. Schwartz and Zhiquan Liu*

NCAR Earth System Laboratory/Mesoscale and Microscale Meteorology Division, Boulder, Colorado, USA

Abstract

As there are few *in situ* observations in and around Antarctica, it is important to assess how assimilating remotely-sensed observations, such as satellite-observed radiances, can fill this observational gap. Thus, a month-long study was conducted over the Antarctic to examine forecast and analysis sensitivity to the assimilation of microwave radiance measurements. Several experiments were configured to quantify the impact of radiance data assimilation (DA) and explore different approaches of radiance bias correction (BC). DA was performed using WRFDA's three-dimensional variational (3DVAR) algorithm, and the analyses initialized 72-hr Advanced Research WRF forecasts.

The results demonstrate the critical importance of properly bias correcting raw radiance observations. When assimilating radiances using a "cold start" BC technique, the maximum benefit from radiance DA was not realized and forecasts and analyses were sometimes degraded compared to when only conventional (i.e., non-radiance) observations were assimilated. However, when BC parameters were "spun-up" for several months before the assimilation period, radiance DA clearly yielded forecast and analysis improvements compared to only assimilating conventional observations.

---

1. Introduction

This study examines how assimilating satellite radiances from microwave sensors with the Weather Research and Forecasting Data Assimilation (WRFDA; Barker et al. 2004) three-dimensional variational (3DVAR) algorithm impacts numerical weather prediction (NWP) analyses and forecasts over the Antarctic. In a 3DVAR system, a best-fit "analysis" is calculated considering two sources of initial information: observations at irregularly spaced points and a background (or "first-guess") field, typically taken to be a short-term, gridded model forecast. Associated with the background and observations are their error characteristics. Given the background, observations, and errors, the analysis ($\mathbf{x}$) can be determined by minimizing a scalar cost-function (J) given by

$$J(\mathbf{x}) = \frac{1}{2}(\mathbf{x}-\mathbf{x_b})^{\mathrm{T}}\mathbf{B}^{-1}(\mathbf{x}-\mathbf{x_b}) + \frac{1}{2}(\mathbf{y}-H(\mathbf{x}))^{\mathrm{T}}\mathbf{R}^{-1}(\mathbf{y}-H(\mathbf{x})) , \tag{1}$$

where $\mathbf{x_b}$ denotes the background, $\mathbf{y}$ is the observations, and $\mathbf{B}$ and $\mathbf{R}$ represent the background and observation error covariance matrices, respectively. H is the potentially

Corresponding author email address: schwartz@ucar.edu

non-linear "observation operator" that interpolates grid-point values to observation locations and transforms model-predicted variables to observed quantities. Eq. (1) is typically linearized about the background field and solved iteratively until the value of **x** is found that minimizes *J*.

Most operational centers currently use variational analysis systems to initialize their NWP models and assimilate microwave radiances[1]. The assimilation of microwave radiances has led to forecast improvements, particularly at intermediate time-ranges (3-7 day forecasts) in global models over areas with few conventional observations[2] (e.g., Caplan et al. 1997; Derber and Wu 1998; Zapotocny et al. 2007, 2008).

However, the impact of radiance data assimilation (DA) within limited-area domains has been less-often studied. Nonetheless, it is important to understand how assimilation of radiances influences regional forecasts, as limited-area and global NWP systems may respond differently to radiance DA due to non-uniform satellite coverage in the former. Moreover, some regional studies have either suggested the forecast impact of radiance assimilation does not persist as long as in a global system (Zapotocny et al. 2005) or found an unclear overall impact (Xu et al. 2009), possibly due to lateral boundary condition (LBC) contamination (Warner et al. 1997).

As there are few *in situ* observations in and around Antarctica, it is important to determine how remotely-sensed observations, such as microwave radiances, can fill this observational gap. Thus, this work examines how radiance DA impacts analyses and forecasts over the Antarctic by performing a month-long sensitivity study. Next, we overview bias correction (BC) of satellite radiances, as this procedure is critical for their successful assimilation. The experimental design is described in section 3. Distributions of the observations are presented in section 4 and results are detailed in section 5 before concluding.

2. Bias correction of satellite radiances

Satellite radiance measurements are prone to systematic errors (i.e., biases) that must be corrected before radiances are assimilated. Even though a NWP system may be biased, most operational centers measure the observation bias with respect to the NWP system itself. There are different methods of BC, but a popular technique is variational bias correction (VarBC), which performs BC as a part of the analysis, thus considering information from conventional observations and the full background field. VarBC is

[1]Satellites sense radiation at known frequencies, so measured radiances can be converted to brightness temperatures by inverting the Planck function. Most operational centers assimilate brightness temperatures rather than raw radiances, and we do the same.

[2] Herein, "conventional observations" means all observations other than microwave radiances.

detailed in Derber and Wu (1998), Dee (2005), and Auligné et al. (2007), but is briefly described here.

In the VarBC approach, a modified observation operator ($\tilde{H}$) is defined that includes corrections to the model-simulated brightness temperatures based on a set of N_p potentially state-dependent predictors (p_i) and their coefficients[3] (β_i):

$$\tilde{H}(\mathbf{x},\beta) = H(\mathbf{x}) + \sum_{i=1}^{N_p} \beta_i p_i(\mathbf{x}). \qquad (2)$$

The cost-function [Eq. (1)] is augmented by adding the predictor coefficients to the state ($\mathbf{x}$), thus introducing a parameter background error covariance matrix ($\mathbf{B}_\beta$). $\mathbf{B}_\beta$ determines how much the updated coefficients are weighted toward the background BC coefficients ($\beta_\mathbf{b}$), which are typically values from a previous cycle. A large $\mathbf{B}_\beta$ means the parameter coefficients update quickly when confronted with new observations.

The inclusion of BC coefficients in the state vector and observation operator leads to a modified cost function that is minimized with respect to both $\mathbf{x}$ and $\boldsymbol{\beta}$:

$$J(\mathbf{x},\beta) = \frac{1}{2}(\mathbf{x}-\mathbf{x_b})^{\mathrm{T}}\mathbf{B}^{-1}(\mathbf{x}-\mathbf{x_b}) + \frac{1}{2}(\beta-\beta_\mathbf{b})^{\mathrm{T}}\mathbf{B}_\beta{}^{-1}(\beta-\beta_\mathbf{b}) + \frac{1}{2}(\mathbf{y}-\tilde{H}(\mathbf{x},\beta))^{\mathrm{T}}\mathbf{R}^{-1}(\mathbf{y}-\tilde{H}(\mathbf{x},\beta)). \quad (3)$$

Minimizing Eq. (3) updates both the meteorological state variables and BC coefficients simultaneously, thus correcting radiance innovations while preserving the fit to other observations.

BC coefficients can also be updated independently of the analysis using an "offline" method (Auligné et al. 2007). In this approach, the following cost-function is minimized:

$$J(\beta) = \frac{1}{2}(\beta-\beta_\mathbf{b})^{\mathrm{T}}\mathbf{B}_\beta{}^{-1}(\beta-\beta_\mathbf{b}) + \frac{1}{2}(\mathbf{y}-\tilde{H}(\mathbf{x_b},\beta))^{\mathrm{T}}\mathbf{R}^{-1}(\mathbf{y}-\tilde{H}(\mathbf{x_b},\beta)). \qquad (4)$$

This equation is similar to the full VarBC expression [Eq. (3)], except there is no term associated with the background field since $\mathbf{x_b}$ is assumed to be good. With this assumption, the background is used as the reference from which model-simulated radiances are calculated, and the observation vector $\mathbf{y}$ only contains radiance observations. The best-fit to Eq. (4) is achieved solely by updating the vector $\boldsymbol{\beta}$. This method adjusts the radiances toward the background and can result in improved estimates of the BC predictor coefficients.

[3] In WRFDA, there were four state-dependent predictors: 1000-300 hPa thickness, 200-50 hPa thickness, surface skin temperature, and total column precipitable water. In addition, several state-independent predictors based on the satellite scanning angle were used.

3. Experimental design

Between 1200 UTC 1 October and 1200 UTC 31 October 2007, several experiments quantified the impact of assimilating microwave radiances over the Antarctic using both cyclic and non-cyclic DA approaches. In the cyclic experiments, the previous analysis cycle's 6-hr forecast served as the background ($\mathbf{x_b}$) for the current analysis, and a new 3DVAR analysis was made at 0000, 0600, 1200, and 1800 UTC during the experimental period.

However, in the non-cyclic experiments, 3DVAR analyses were only produced at 0000 and 1200 UTC. The backgrounds for DA came from 6-hr Advanced Research WRF (ARW; Skamarock et al. 2008) forecasts initialized at either 0600 or 1800 UTC. In turn, the initial conditions (ICs) for the 0600 and 1800 UTC ARW forecasts came from NCEP's Global Forecast System (GFS) analyses interpolated onto the computational domain (Fig. 1). In general, we expect cyclic experiments to yield more differences among themselves due to the impact of data accumulation throughout the cycles, but non-cyclic ICs provides a cleaner indication of data impact, since each experiment uses the same background each analysis.

A 72-hr ARW forecast was initialized from each 0000 and 1200 UTC analysis for all experiments.

Within *both* the cyclic and non-cyclic sets, three experiments were performed that differed in terms of the observations they assimilated and/or radiance BC approach. The first experiment (conv) assimilated only conventional observations. The other two experiments assimilated microwave radiances from Advanced Microwave Sounding Unit A and B (AMSU-A, AMSU-B) and Microwave Humidity Sounder (MHS) sensors outfitted on polar orbiting satellites but differed in their specifications of the initial BC predictor coefficients. For example, one experiment (conv+RAD_spin_up) assimilated conventional and radiance observations and used initial BC coefficients that were generated by performing offline analyses every 6-hrs for three months (July-September 2007) using ERA-Interim reanalyses (Dee et al. 2011) as reference fields, where the background BC parameters ($\beta_\mathbf{b}$) for each cycle were inherited from the previous cycle. Conversely, a parallel experiment (conv+RAD) assimilated the same conventional and radiance observations but used an initial set of BC coefficients that were *not* spun-up beforehand (hereafter "cold-start BC coefficients"). The experimental configurations are summarized in Table 1 and the satellites that were used for radiance DA are listed in Table 2.

Note that all experiments (cyclic and non-cyclic) assimilating radiances cycled the predictor coefficients each analysis *during* the experimental period—that is, $\boldsymbol{\beta}$ was updated each analysis with the full VarBC algorithm [(Eq. (3)] using the previous cycle's coefficients as the background ($\beta_\mathbf{b}$).

Experiment name	Radiances assimilated?	Initially spun-up BC coefficients?	Cyclic DA?
conv	NO	N/A	NO
conv+RAD	YES	NO	NO
conv+RAD_spin_up	YES	YES	NO
cyc_conv	NO	N/A	YES
cyc_conv+RAD	YES	NO	YES
cyc_conv+RAD_spin_up	YES	YES	YES

Table 1. Summary of the experiments.

Satellite	Sensors	Channels
NOAA-15	AMSU-A	5-9
NOAA-16	AMSU-A	5-8
NOAA-17	AMSU-B	3,5
NOAA-18	AMSU-A,MHS	AMSU-A: 5-8; MHS: 3-5
METOP-2	AMSU-A, MHS	AMSU-A: 5,6,8,9; MHS: 3-5

Table 2. Satellites, sensors, and channels that were assimilated.

Aside from assimilating different observations and varying the initial BC coefficients, the experiments were otherwise configured identically, thus permitting a clear assessment of the impact of radiance DA within cyclic and non-cyclic frameworks. For example, all experiments were integrated over the same computational domain (Fig. 1). The horizontal grid spacing was 45-km. There were 44 vertical levels and the model top was 10 hPa. Observations within 1.5 hours of the analysis times were assimilated. Radiances were thinned on a 90-km mesh grid and assimilated for non-precipitating pixels only. The Community Radiative Transfer Model (CRTM) was used to calculate model-simulated brightness temperatures and the GFS provided LBCs.

4. Observation coverage

DA over the Antarctic is challenging due to few *in situ* observations in the region. Fig. 2 shows a representative snapshot of non-radiance observations available for assimilation over the computational domain at 0000 UTC 2 October. There were a handful of soundings (Fig. 2b) and a fair amount of surface observations (Fig. 2d) taken over the Antarctic continent. But, aside from a few Global Positioning System radio occultation (GPS-RO) profiles (Fig. 2a), there were virtually no upper-air or surface observations over the sea (Fig. 2c).

Fortunately, satellite coverage over the domain was very good (Fig. 3) and copious radiance observations were assimilated every cycle (Fig. 4). The experiments that used initially spun-up BC coefficients assimilated more radiances each analysis than the experiments using cold-start predictor coefficients. As the background fields were constant for all experiments in the non-cyclic configurations, the different number of assimilated radiances was entirely due to better estimates of the BC coefficients generated during the offline spin-up, which led to smaller innovations and fewer rejections.

5. Results

As radiance DA is designed to generally make small corrections to the first-guess, it was difficult to discern visual differences among the experiments regarding individual forecasts. Thus, we focus on statistics aggregated over all initializations. Additionally, since there were few sounding sites against which to perform verification, analyses and forecasts were mostly compared to ERA-Interim reanalyses interpolated onto the computational domain and considered as "truth." We examine the non-cyclic experiments before evaluating the cyclic experiments.

a. Non-cyclic experiments

At the analysis time, domain-wide aggregate root-mean-square-errors (RMSEs; Fig. 5) reveal substantial differences between the non-cyclic experiments. When radiances were assimilated with initial cold-start BC coefficients, the analyses were degraded, especially for low- and upper-level wind (Fig. 5a,d,f), but also for low- and mid-level temperature (Fig. 5b). But, above ~150 hPa, the addition of radiances—even without initially spun-up BC coefficients—improved analyses of geopotential height and temperature (Fig. 5b,e).

On average, the best analyses occurred when radiances were assimilated using initially spun-up BC coefficients. Temperature analyses below ~850 hPa and wind analyses between ~500-250 hPa were improved with radiance DA. Height analyses were improved above 300 hPa. Moisture analyses (Fig. 5c) were insensitive to assimilating radiances.

The spatial characteristics of the mean 500 hPa temperature analysis increments also demonstrate the impact of radiance DA. Without assimilating radiances (Fig. 6a) large increments were generated over Antarctica and the ocean on the western-hemispheric side of the continent. However, with radiance DA (Fig. 6b) the increments were much smaller. These different increment structures were also reflected in the spatial distribution of the average 500 hPa temperature RMSE at the initial time (again compared to ERA-Interim reanalyses). Although the aggregate RMSE (Fig. 5b) showed little difference between the two experiments at this level, examining a map of the errors reveals large differences (Fig 7). Radiance DA (Fig. 7b) led to much lower RMSEs over the sea, particularly over the region where the analysis increments were smaller (see Fig. 6). Over the continent, assimilating radiances produced larger RMSEs in some areas but lower RMSEs in others.

There were also differences in the initial wind fields. As microwave radiance measurements are not impacted by wind, differences at the analysis time among the experiments arise due to multivariate background error correlations between the mass and velocity fields. Aggregate RMSEs for 500 hPa wind components (Fig. 8) show that the inclusion of radiances yielded lower RMSEs over the ocean, particularly for the meridional wind component (Fig. 8c,d) but also the zonal wind (Fig. 8a,b). Compared to the RMSEs over the sea, RMSEs were lower over Australia and the eastern side of Antarctica where several soundings were launched (see Fig. 2b), underscoring the value of soundings to DA and NWP systems.

The different ICs produced subsequently different forecasts. The experiment that assimilated radiances using initially spun-up BC coefficients produced improved 12-hr wind forecasts between ~250-500 hPa compared to when radiances were not assimilated or radiances were assimilated with cold-start BC coefficients (Fig. 9a,d,f). Additionally, 12-hr temperature (height) forecasts above ~150 hPa (~100 hPa) were improved by radiance DA when the initial BC coefficients were spun-up (Fig. 9b,e). A slight improvement of 12-hr moisture forecasts below 925 hPa was also noted in the experiment assimilating radiances with spun-up BC coefficients (Fig. 9c). When the initial BC coefficients were not spun-up, forecasts of wind and low-level temperature and moisture were degraded. Again, although the domain-wide statistics revealed no major differences, a map of the average RMSE of 12-hr 500 hPa temperature forecasts (Fig. 10) shows that RMSEs over the sea were substantially reduced when radiances were assimilated with initially spun-up BC coefficients.

For 24-hr forecasts (Fig. 11), the experiment assimilating radiances with cold-start BC coefficients produced the worst forecasts of wind and low-level moisture. Wind forecasts were improved in a small mid-level layer (Fig. 11a,d,f) when radiances were assimilated with spun-up BC coefficients. This improvement was also evident in 48-hr wind forecasts between 300-400 hPa (Fig. 12). Otherwise, by 48-hrs, there were no differences among the three non-cyclic experiments.

Overall, low-level temperature, mid-level wind, and upper-level height analyses were improved by assimilating radiances using initially spun-up BC coefficients. Short-term wind forecasts were also improved slightly when radiances were assimilated with initially spun-up BC coefficients, but assimilating radiances with cold-start initial BC coefficients degraded the forecasts compared to when just conventional observations were assimilated. However, all the differences between the experiments were small. Verification was also performed against GFS analyses, and very similar results were obtained (not shown).

b. Cyclic experiments

As expected, cyclic DA yielded much larger differences among the experiments. At most levels, assimilating radiances both with initially spun-up and cold-start BC coefficients produced better analyses of wind (Fig. 13,a,d,f) compared to when radiances were not assimilated. The best analyses were produced when radiances were assimilated using initially spun-up BC coefficients. Similar to the non-cyclic experiments, assimilating radiances primarily improved the 500 hPa temperature analyses over the sea (Fig. 14).

For 12-, 24-, and 48-hr forecasts (Figs. 15-17), radiance DA with initially spun-up BC coefficients produced the best wind forecasts for all variables and levels. Radiance DA also improved temperature and height forecasts, although there was less sensitivity to whether the initial BC coefficients were spun-up. Again, verification was also performed against GFS analyses, and very similar results were obtained (not shown).

When output from the cyclic experiments was compared to all available radiosonde observations within the domain, the results were consistent with verification against ERA-Interim reanalyses. The analysis fits to radiosondes (Fig. 18) were similar for the three cyclic experiments below ~200 hPa. Above ~200 hPa, temperature fits (Fig. 18c) were improved when radiances were assimilated and wind analyses were bettered near the model top (Fig. 18a,b). At the analysis time, there was little sensitivity to whether the initial BC coefficients were spun-up.

For 24-hr forecasts, more differences were evident. Assimilating radiances improved 24-hr wind (Fig. 19a,b) and temperature (Fig. 19c) forecasts at most levels, and 24-hr forecasts of low-level moisture (Fig. 19d) were also improved. Spinning-up the initial BC coefficients produced the best forecasts of mid-tropospheric wind and low-level moisture, but 24-hr temperature forecasts were insensitive to the initial BC coefficients. RMSEs at 48-hrs (Fig. 20) were similar to those at 24-hrs.

Overall, when cyclic DA was performed, assimilating radiances produced a larger impact to both mass and velocity fields compared to the impact using non-cyclic ICs. However, the analyses and forecasts were degraded by cycling, as measured by higher RMSEs. It is also interesting that failing to spin-up the initial BC coefficients degraded the forecasts compared to when only conventional observations were assimilated in the non-cyclic experiments but not in the cyclic configurations.

6. Summary

A series of experiments was conducted to determine the impact of microwave radiance DA over the Antarctic. 3DVAR analyses were performed over October 2007 using both cyclic and non-cyclic DA approaches. Each 0000 and 1200 UTC 3DVAR analysis initialized a 72-hr ARW forecast.

The experimental configurations permitted a clean isolation of the impact of radiance DA in both cyclic and non-cyclic frameworks. On average, when radiance BC coefficients were initialized with values derived from three months of spin-up, assimilating radiances improved analyses and 12-hr forecasts of mid-level wind, upper-level height, and low- and upper-level temperature. In particular, 500 hPa analyses and 12-hr forecasts of temperature were substantially improved over the ocean. In the non-cyclic experiments, once the forecasts integrated to 24- and 48-hrs, there was little difference between the experiments. However, when cyclic ICs were used, a positive impact from radiance DA was clearly evident through 48-hrs.

When radiances were assimilated with cold-start BC coefficients, analyses and 12-hr forecasts were degraded for nearly all meteorological variables in the non-cyclic experiments. Additionally, an improvement was noted in the cycling experiments when the initial BC coefficients were spun-up compared to when they were not. Based on these findings, it is advisable to spin-up the BC predictor coefficients using an offline method for at least a month before assimilating radiances. Failure to do so may result in degraded analyses and the adverse impact can be carried through to short-range forecasts.

Acknowledgements

NCAR is sponsored by the National Science Foundation. This work was supported by NSF contract ANT-0839068.

References

Auligné T., A. P. McNally, and D. P. Dee, 2007: Adaptive bias correction for satellite data in a numerical weather prediction system. *Quart. J. Roy. Meteor. Soc.*, **133,** 631–642.

Barker, D. M., W. Huang, Y-R. Guo, A. Bourgeois, and X. N. Xio, 2004: A three-dimensional variational data assimilation system for MM5: Implementation and initial results. *Mon. Wea. Rev.*, **132,** 897–914.

Caplan, P., J. Derber, W. Gemmill, S. Y. Hong, H. L. Pan, and D. Parish, 1997: Changes to the 1995 NCEP operational medium-range forecast model analysis–forecast system. *Wea. Forecasting*, **12,** 581–594.

Dee, D. P., 2005: Bias and data assimilation. *Quart . J. Roy. Meteor. Soc.*, **131**, 3323–3343.

Dee, D. P., and Coauthors, 2011: The ERA-Interim reanalysis: configuration and performance of the data assimilation system. *Quart. J. Roy. Meteor. Soc.*, **137**, 553–597, DOI:10.1002/qj.828.

Derber, J. C. and W-S. Wu, 1998: The use of TOVS cloud-cleared radiances in the NCEP SSI analysis system. *Mon. Wea. Rev.*, **126,** 2287–2299.

Skamarock, W. C., J. B. Klemp, J. Dudhia, D. O. Gill, D. M. Barker, M. G. Duda, X-Y. Huang, W. Wang, and J. G. Powers, 2008: A description of the Advanced Research WRF version 3. NCAR Tech Note NCAR/TN-475+STR, 113 pp. [Available from UCAR Communications, P. O. Box 3000, Boulder, CO 80307.]

Warner, T. T., R. A. Peterson, and R. E. Treadon, 1997: A tutorial on lateral boundary conditions as a basic and potentially serious limitation to regional numerical weather prediction. *Bull. Amer. Meteor. Soc.*, **78,** 2599–2617.

Xu, J, S. Rugg, L. Byerle, and Z. Liu, 2009: Weather forecasts by the WRF-ARW model with the GSI data assimilation system in the complex terrain areas of Southwest Asia. *Wea. Forecasting*, **24,** 987-1008.

Zapotocny, T. H., W. P. Menzel, J. A. Jung, and J. P. Nelson III, 2005: A four-season impact study of rawinsonde, GOES, and POES data in the Eta Data Assimilation System. Part II: Contribution of the components. *Wea. Forecasting*, **20,** 178–198.

Zapotocny, T. H., J. A. Jung, J. F. Le Marshall, and R. E. Treadon, 2007: A two-season impact study of satellite and in situ data in the NCEP Global Data Assimilation System. *Wea. Forecasting*, **22,** 887–909.

Zapotocny, T. H., J. A. Jung, J. F. Le Marshall, and R. E. Treadon, 2008: A two-season impact study of four satellite data types and rawinsonde data in the NCEP

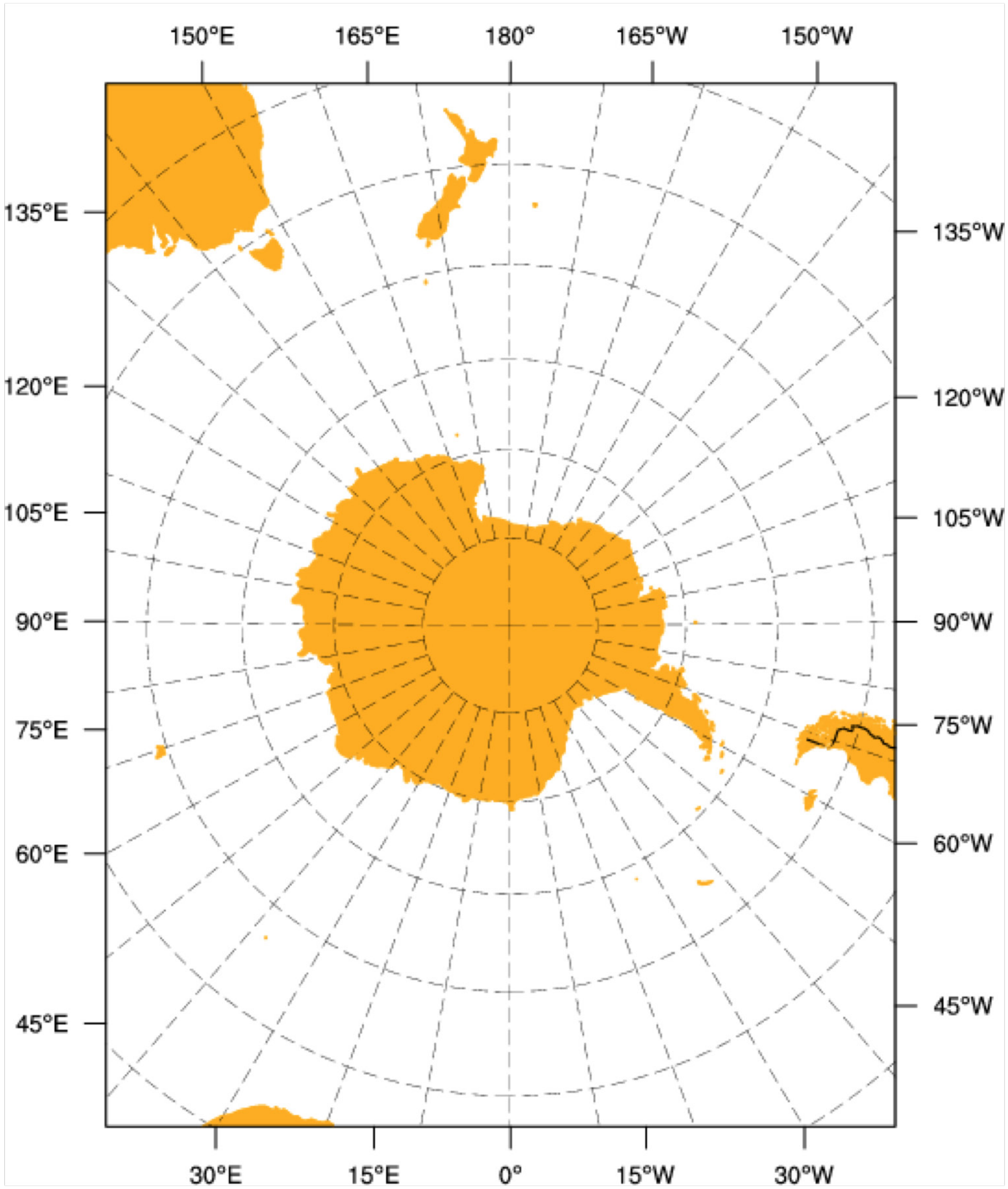

Fig. 1. Computational domain used for all experiments.

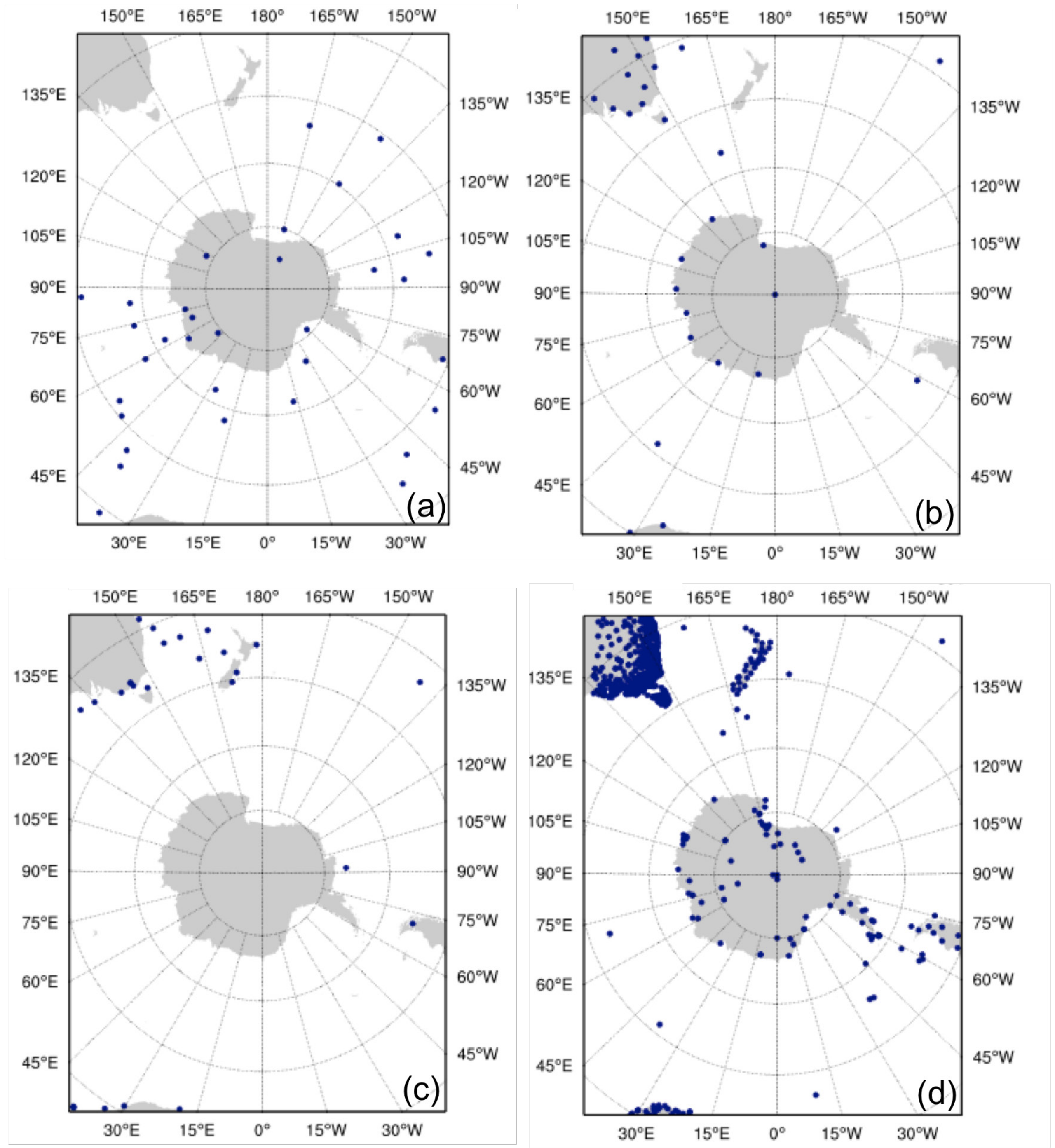

Fig. 2. Snapshot of (a) GPS-RO, (b) sounding, (c) ship, and (d) synop observations available for assimilation for the 0000 UTC 2 October analysis.

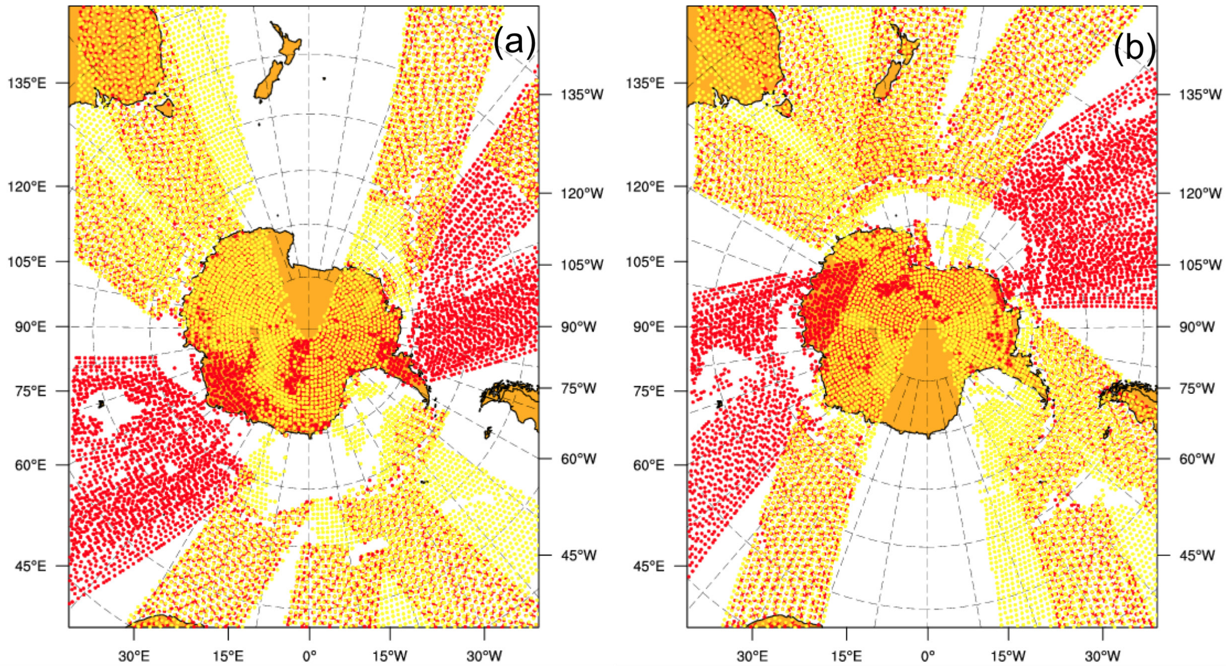

Fig. 3. Spatial distribution of radiances that were actually assimilated during the (a) 0000 UTC 5 October and (b) 1200 UTC 5 October analyses. Red dots represent observations from AMSU-A sensors and yellow dots observations from AMSU-B or MHS sensors.

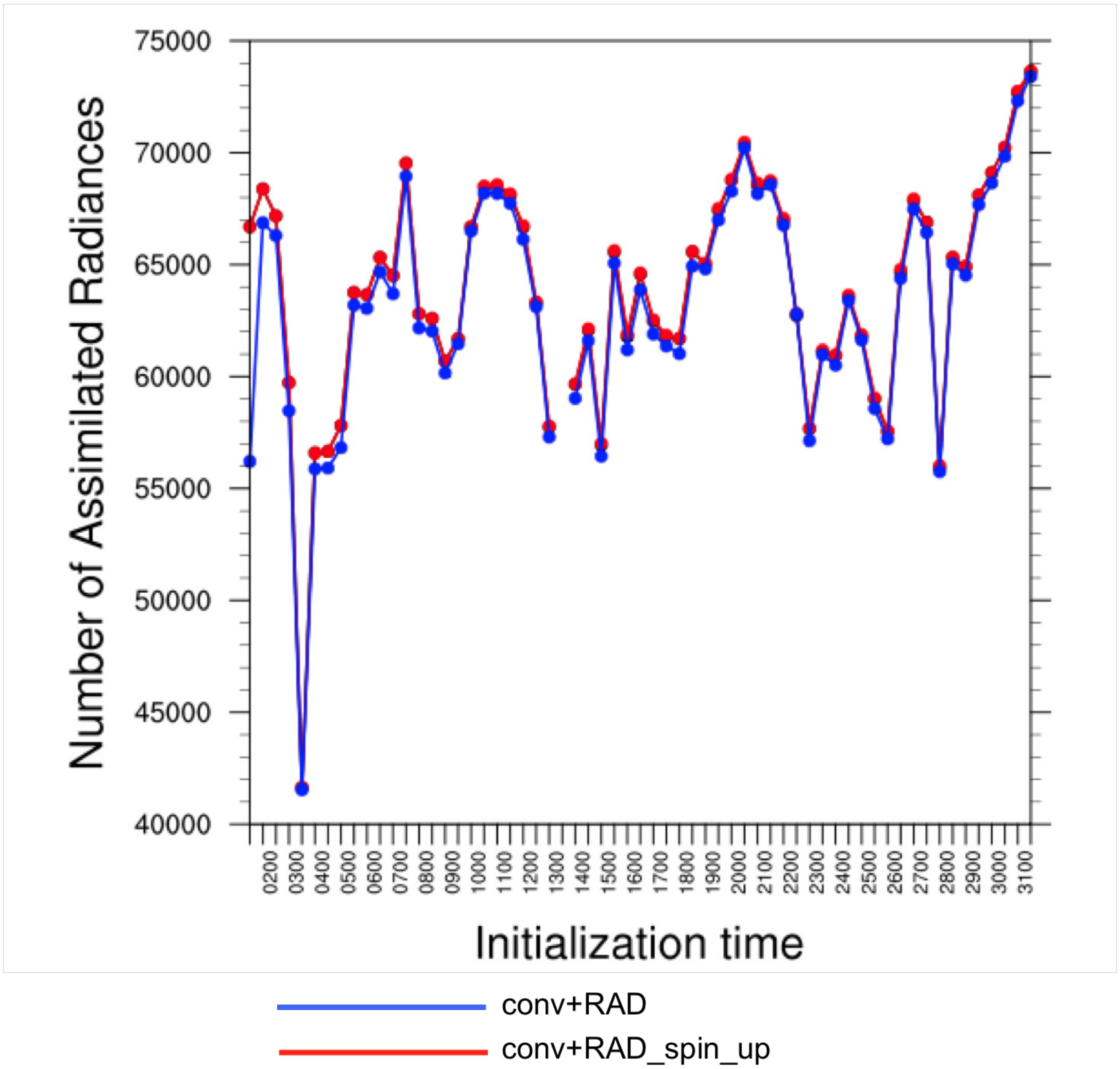

Fig. 4. Number of radiances actually assimilated each analysis for the non-cyclic experiments using initially spun-up BC coefficients (conv+RAD_spin_up; red line) and cold-start BC coefficients (conv+RAD; blue line).

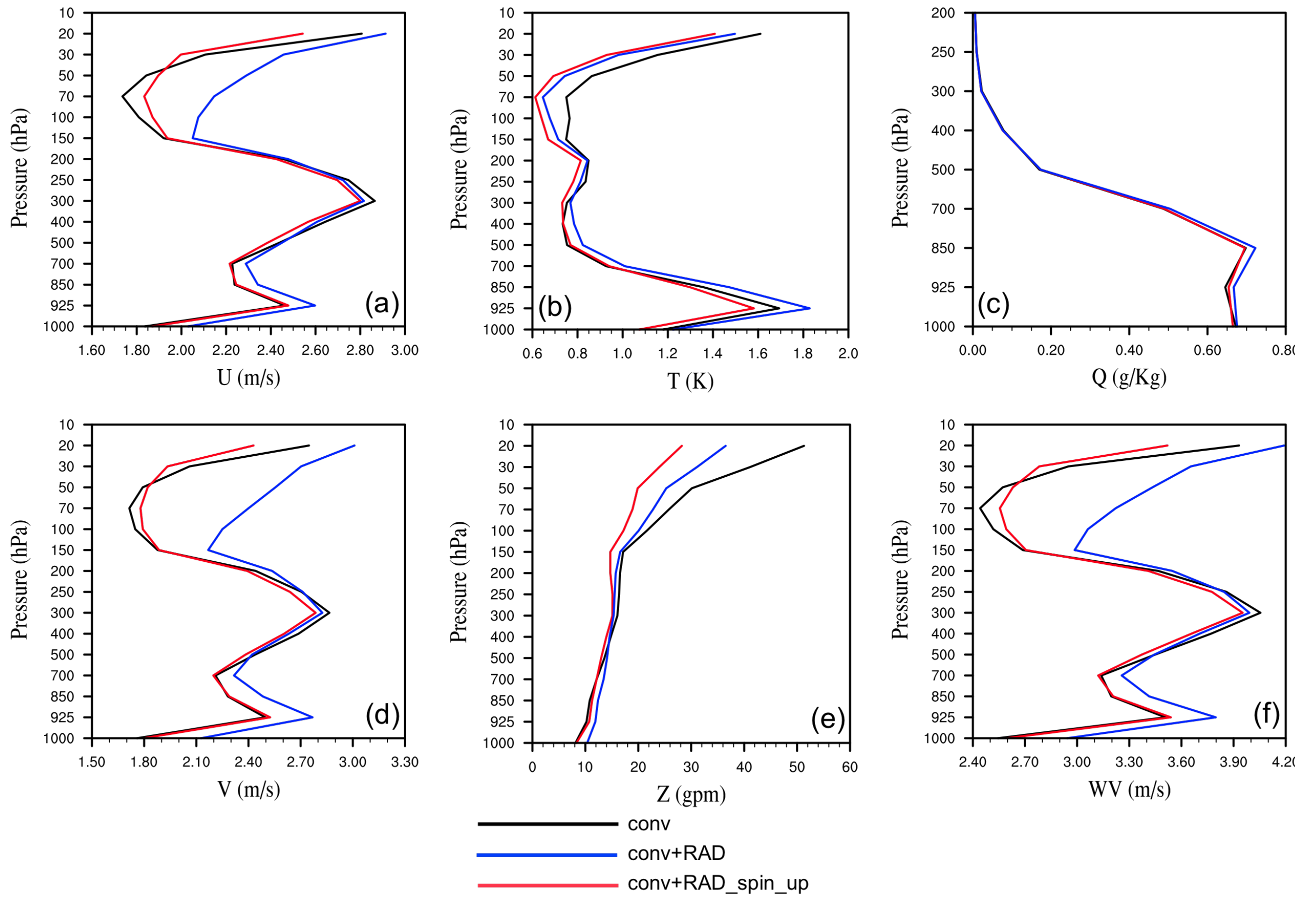

Fig. 5. Domain-wide RMSE aggregated over all initializations for the analysis time. Meteorological variables and their units are specified on the figures: U—zonal wind component; V—meridional wind component; T—temperature; Q—water vapor mixing ratio; Z—geopotential height; WV—wind vector. The wind vector RMSE is calculated as $RMSE_{WV} = \sqrt{(u_m - u_{ref})^2 + (v_m - v_{ref})^2}$, where the subscripts "m" and "ref" refer to the model and reference fields (i.e., ERA-Interim reanalyses), respectively. The curves are for the non-cyclic experiments.

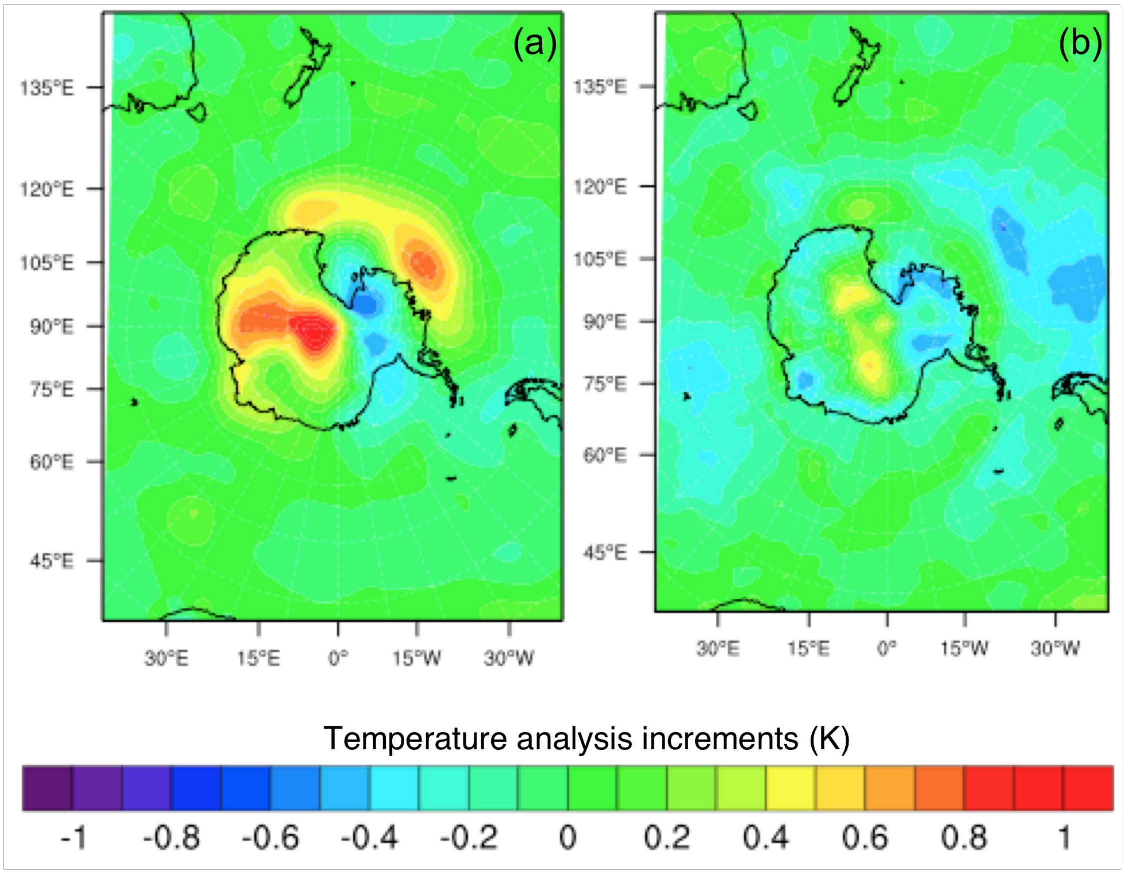

Fig. 6. Average analysis increments of 500 hPa temperature for (a) the non-cyclic experiment that only assimilated conventional observations (conv) and (b) the non-cyclic experiment that assimilated radiances in addition to conventional observations (conv+RAD_spin_up).

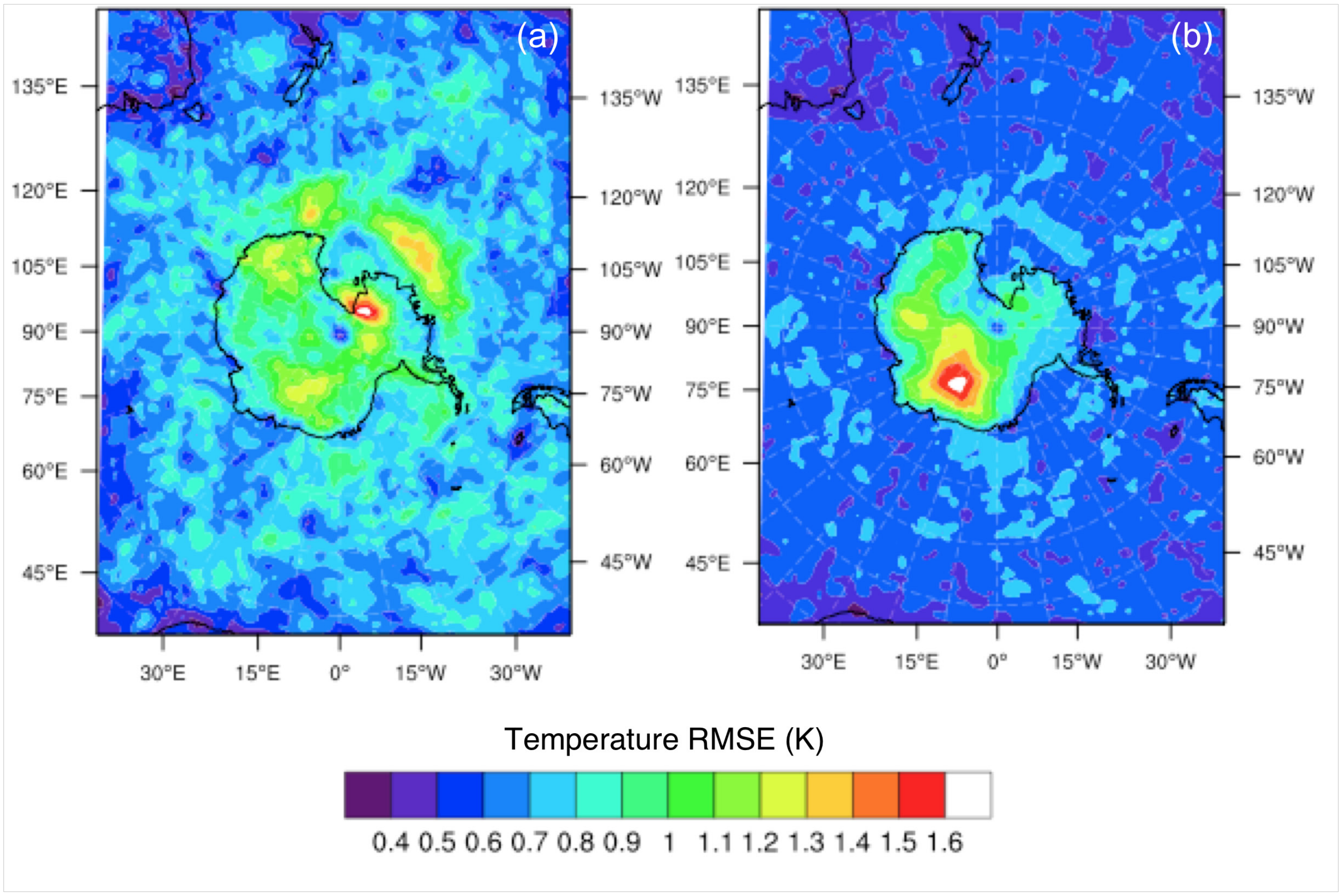

Fig. 7. As in Fig. 6, except the aggregate RMSE of 500 hPa temperature at the initial time is plotted.

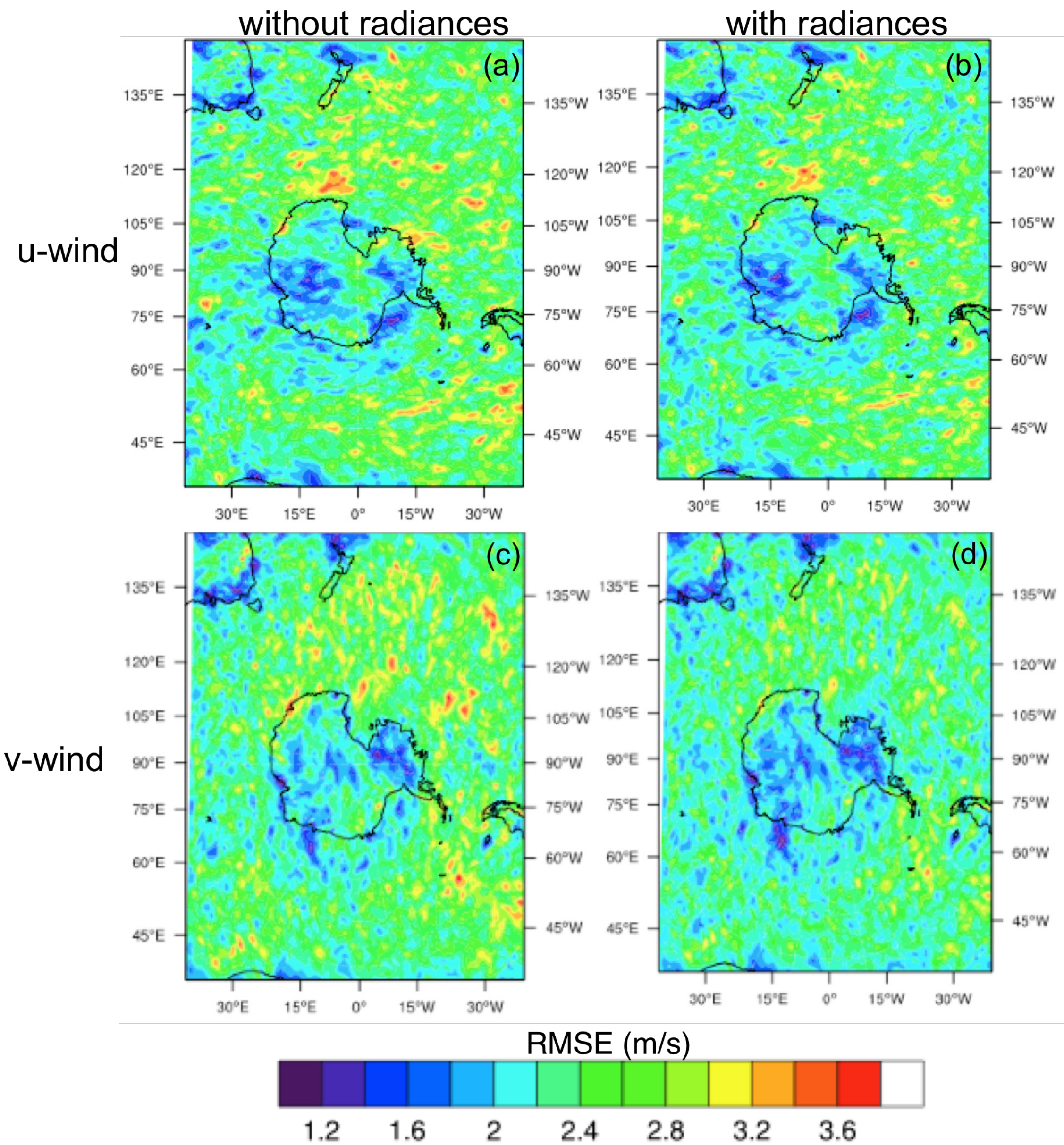

Fig. 8. Average analysis increments of 500 hPa (a)-(b) zonal wind and (c)-(d) meridional wind for the non-cyclic experiment that assimilated radiances in addition to conventional observations (conv+RAD_spin_up; right column) and the non-cyclic experiment that only assimilated conventional observations (conv; left column).

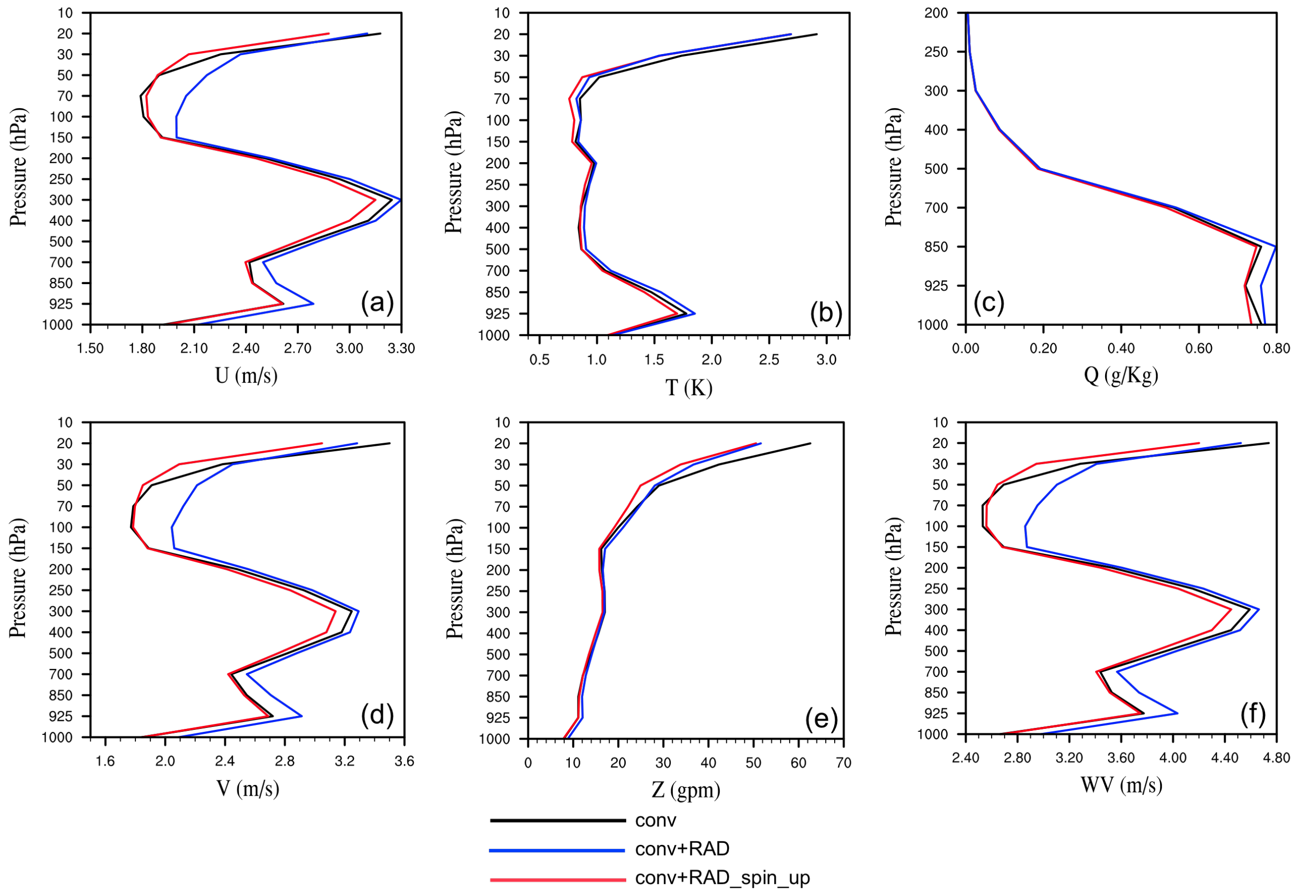

Fig. 9. As in Fig. 5, except the aggregate RMSE of 12-hr forecasts is plotted.

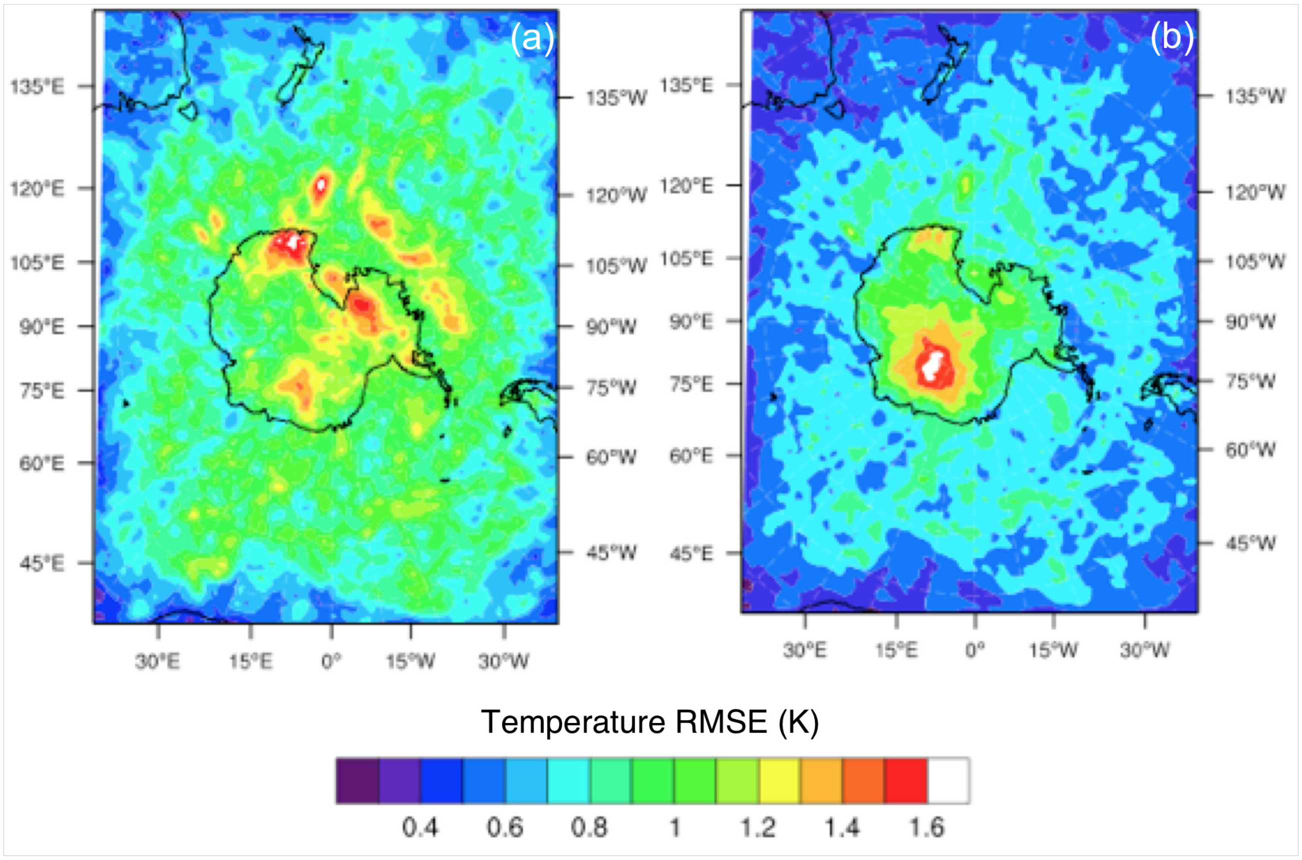

Fig. 10. As in Fig. 7, except the aggregate RMSE of 12-hr forecasts is plotted.

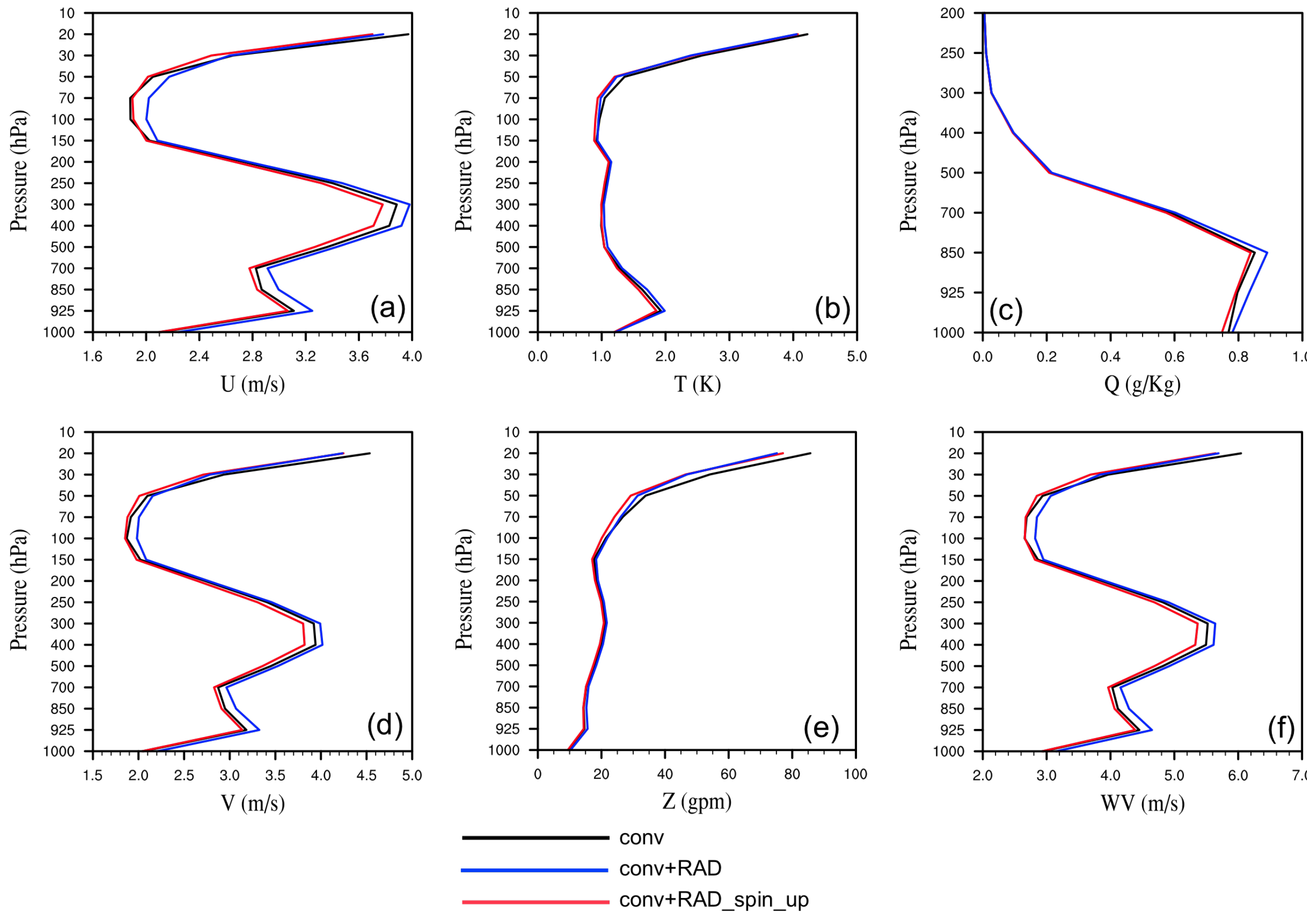

Fig. 11. As in Fig. 5, except the aggregate RMSE of 24-hr forecasts is plotted.

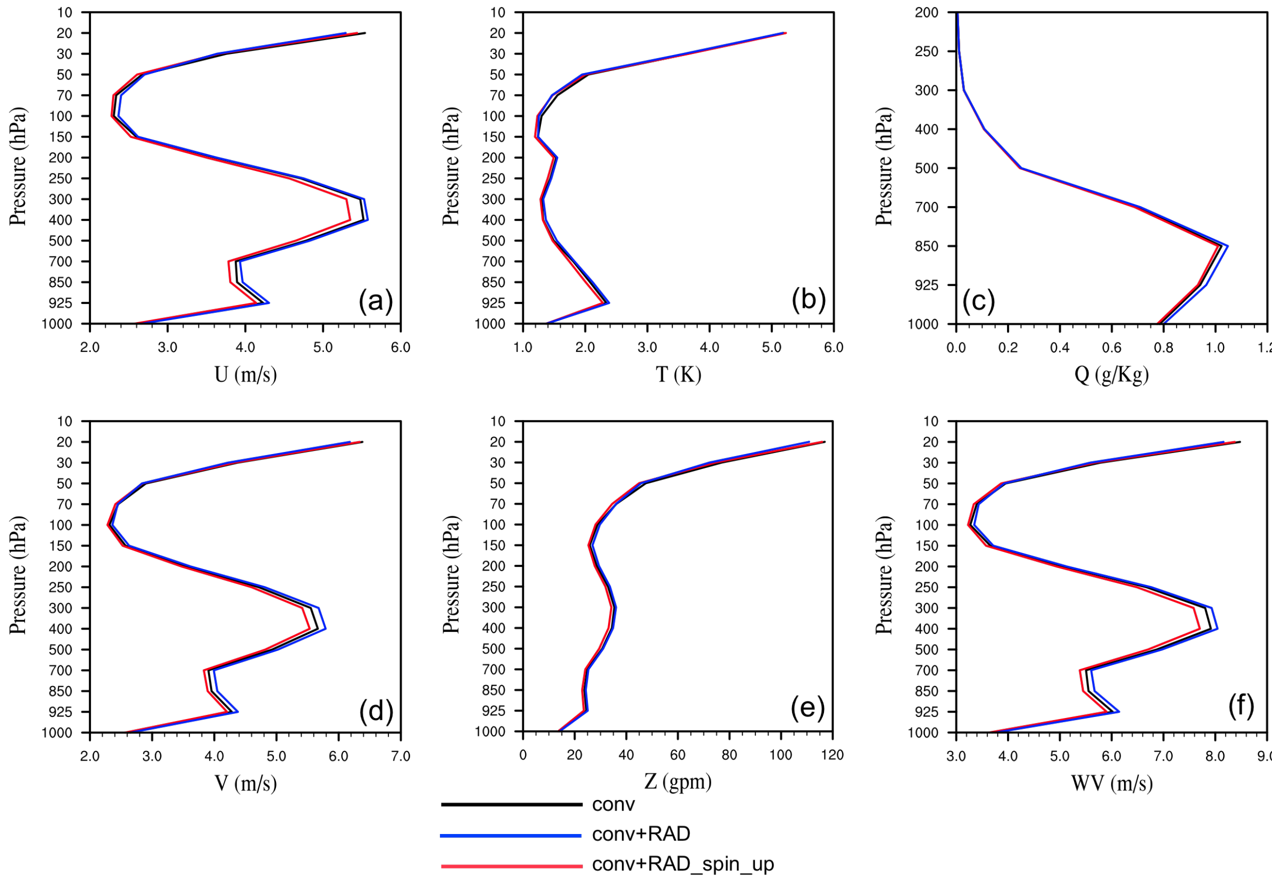

Fig. 12. As in Fig. 5, except the aggregate RMSE of 48-hr forecasts is plotted.

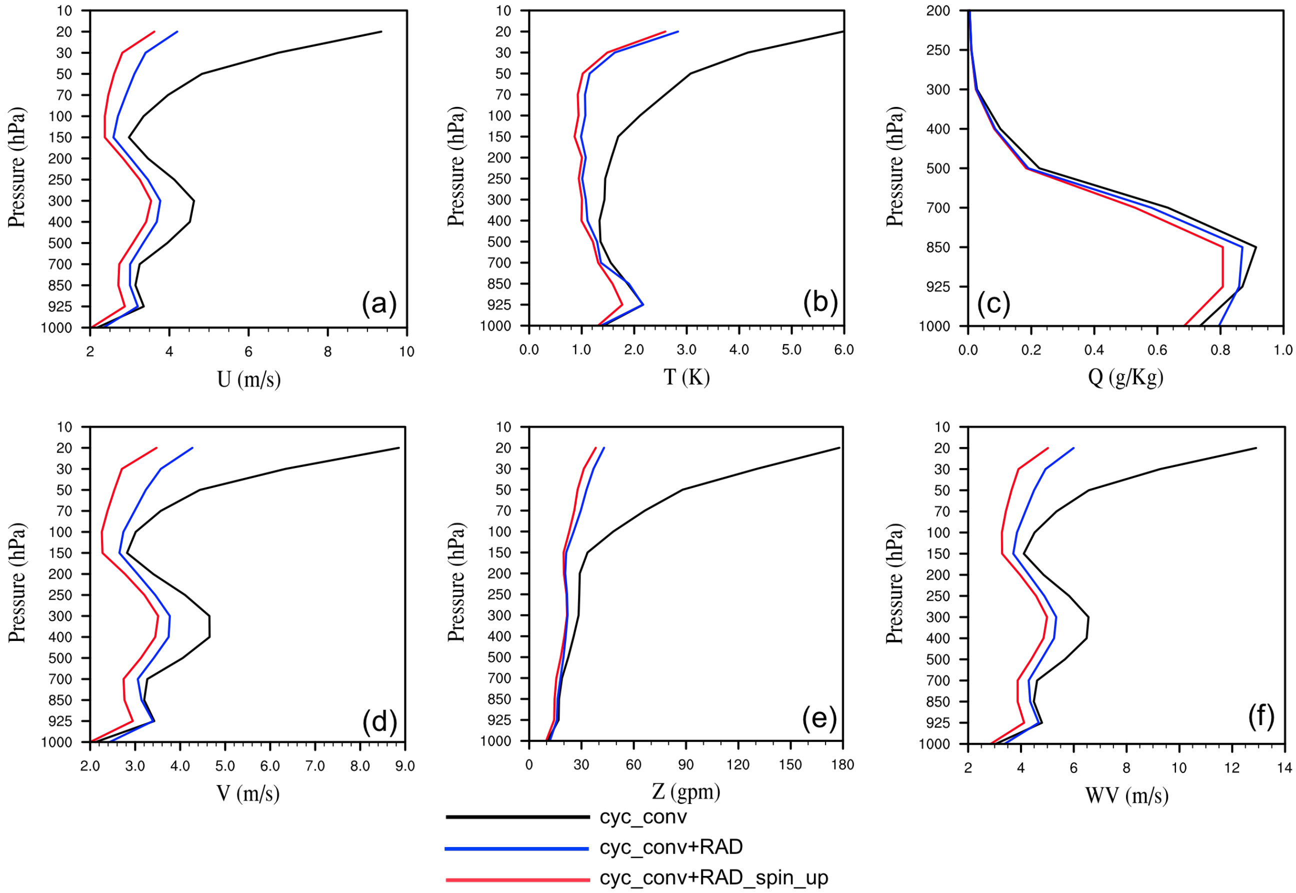

Fig. 13. As in Fig.5, but for the cycling experiments: Domain-wide RMSE aggregated over all initializations for the analysis time.

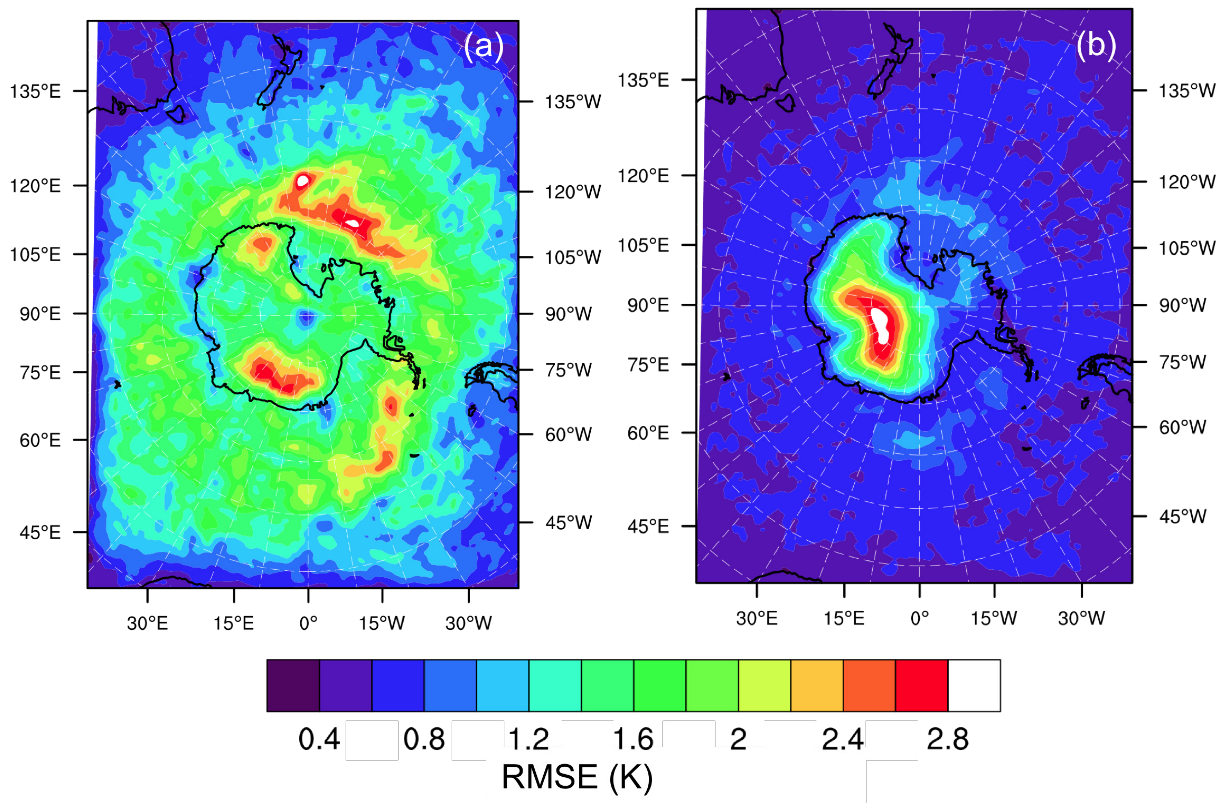

Fig. 14. As in Fig. 7, but for the cycling experiments: aggregate RMSE of 500 hPa temperature at the initial time for (a) the cyclic experiment that only assimilated conventional observations (cyc_conv) and (b) the cyclic experiment that assimilated radiances in addition to conventional observations (cyc_conv+RAD_spin_up)

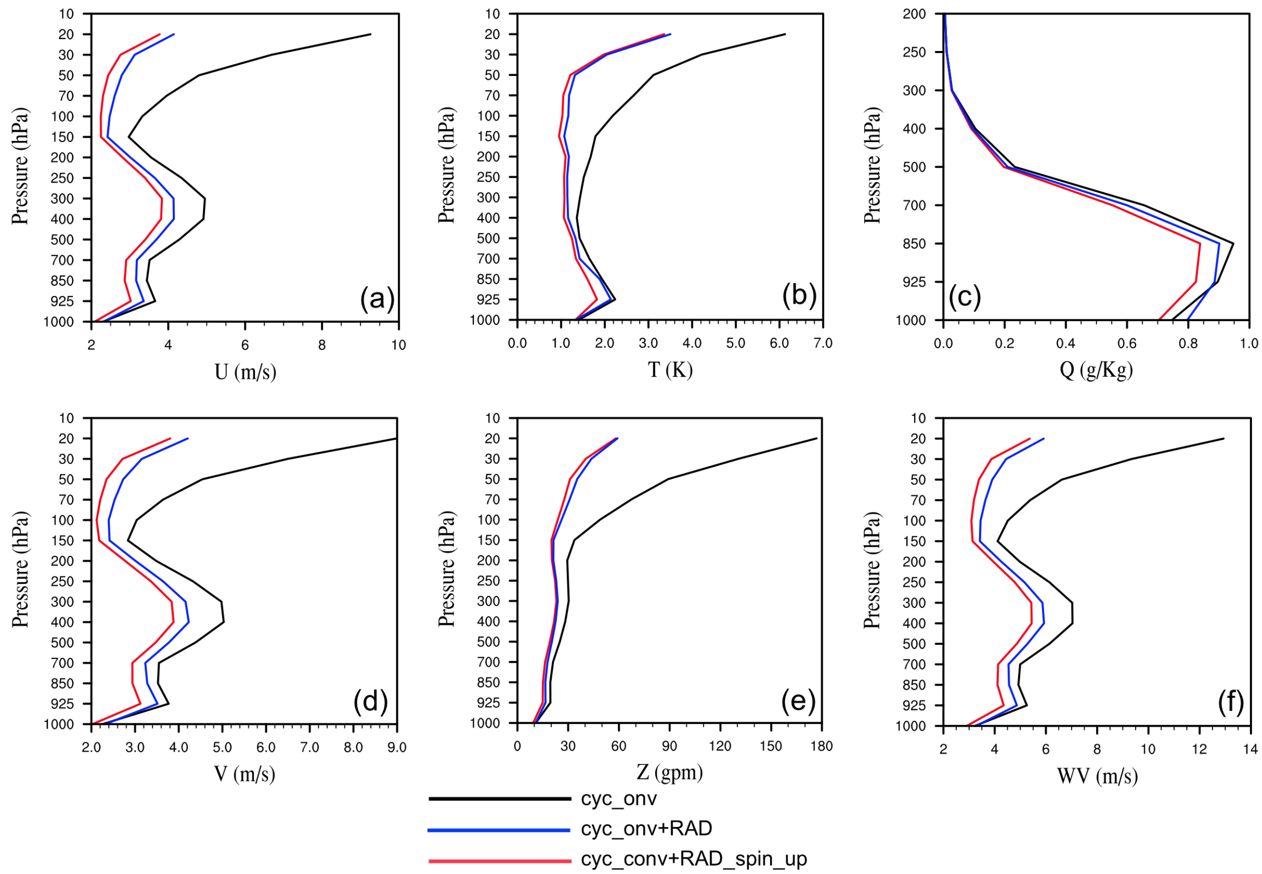

Fig. 15. As in Fig.13, except the aggregate RMSE of 12-hr forecasts is plotted.

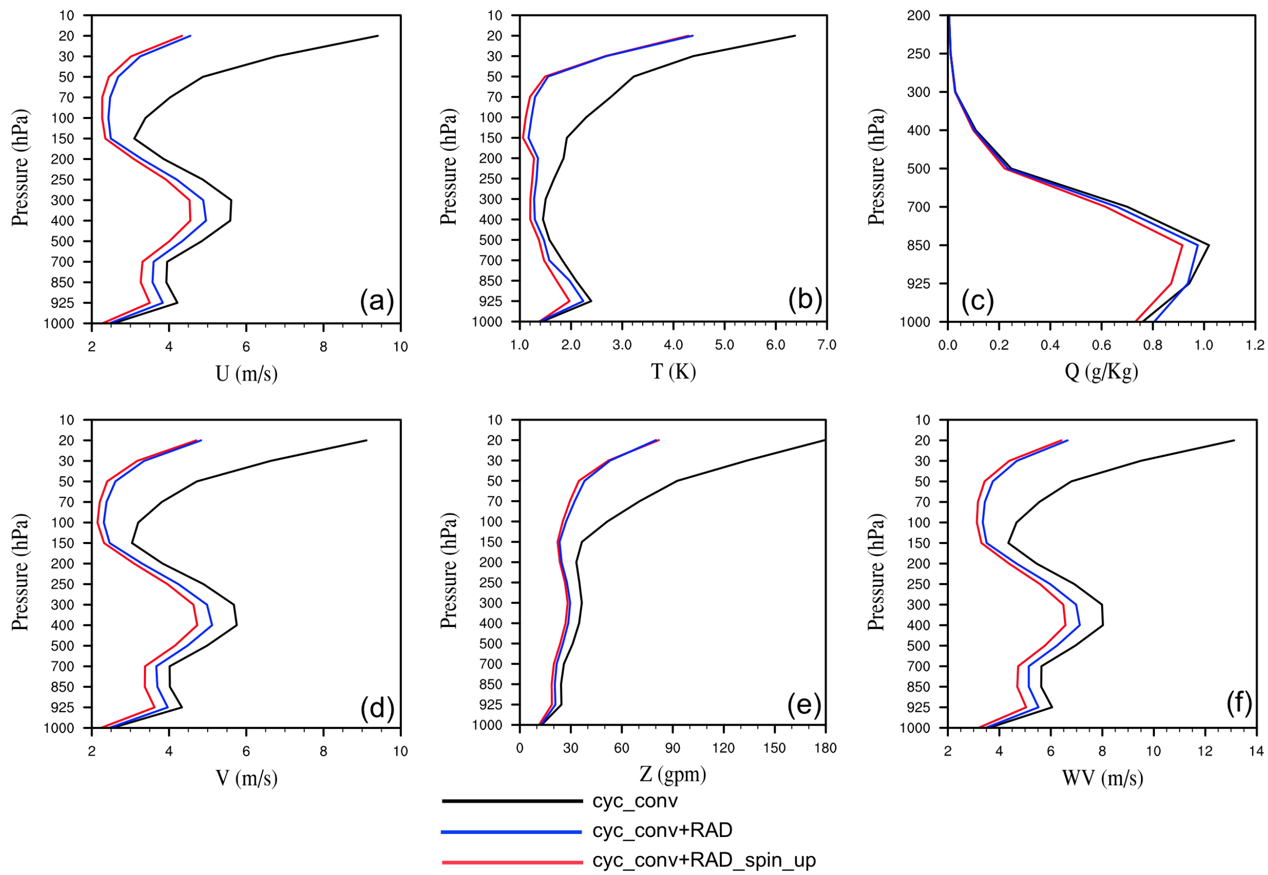

Fig. 16. As in Fig.13, except the aggregate RMSE of 24-hr forecasts is plotted.

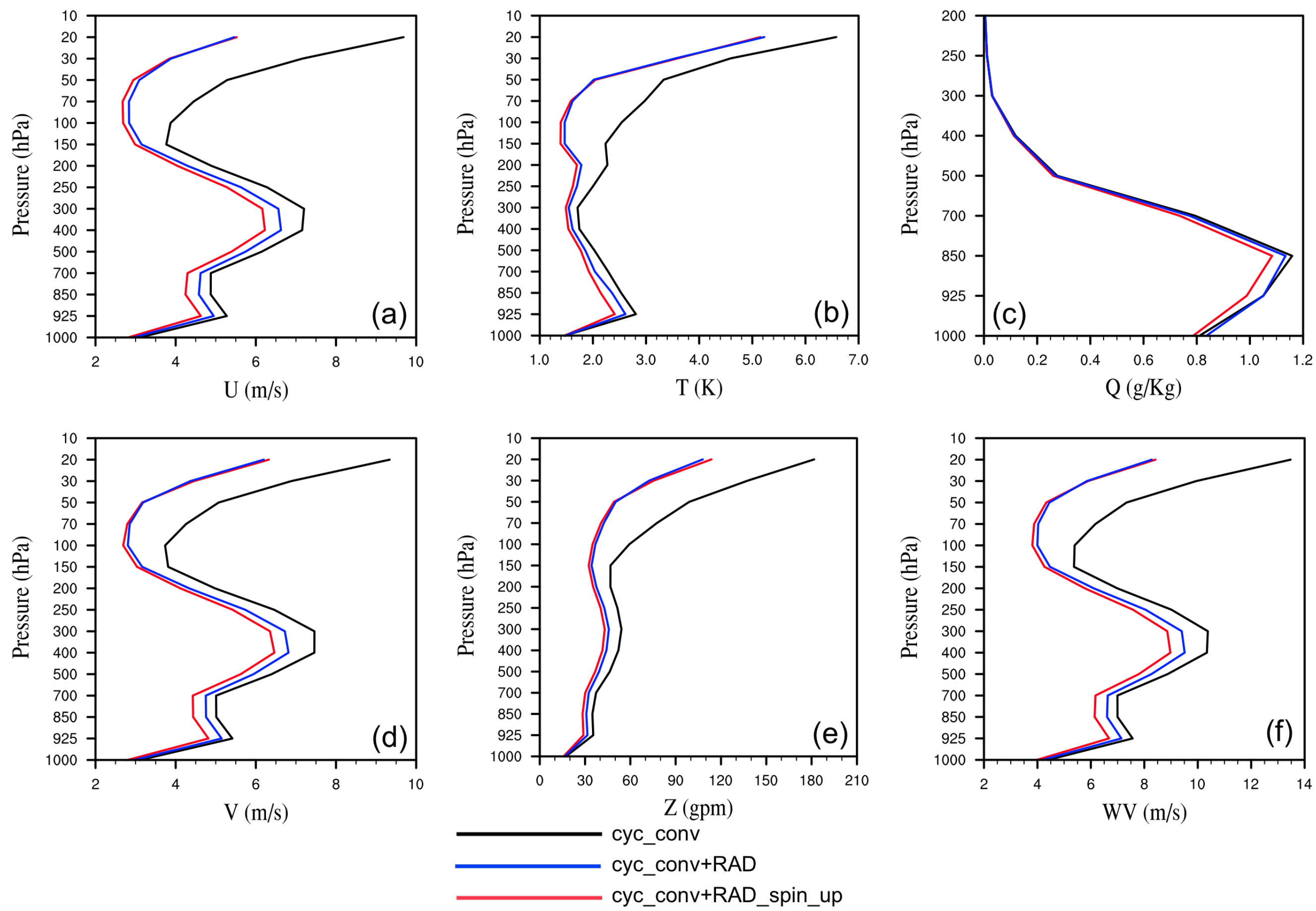

Fig. 17. As in Fig.13, except the aggregate RMSE of 48-hr forecasts is plotted.

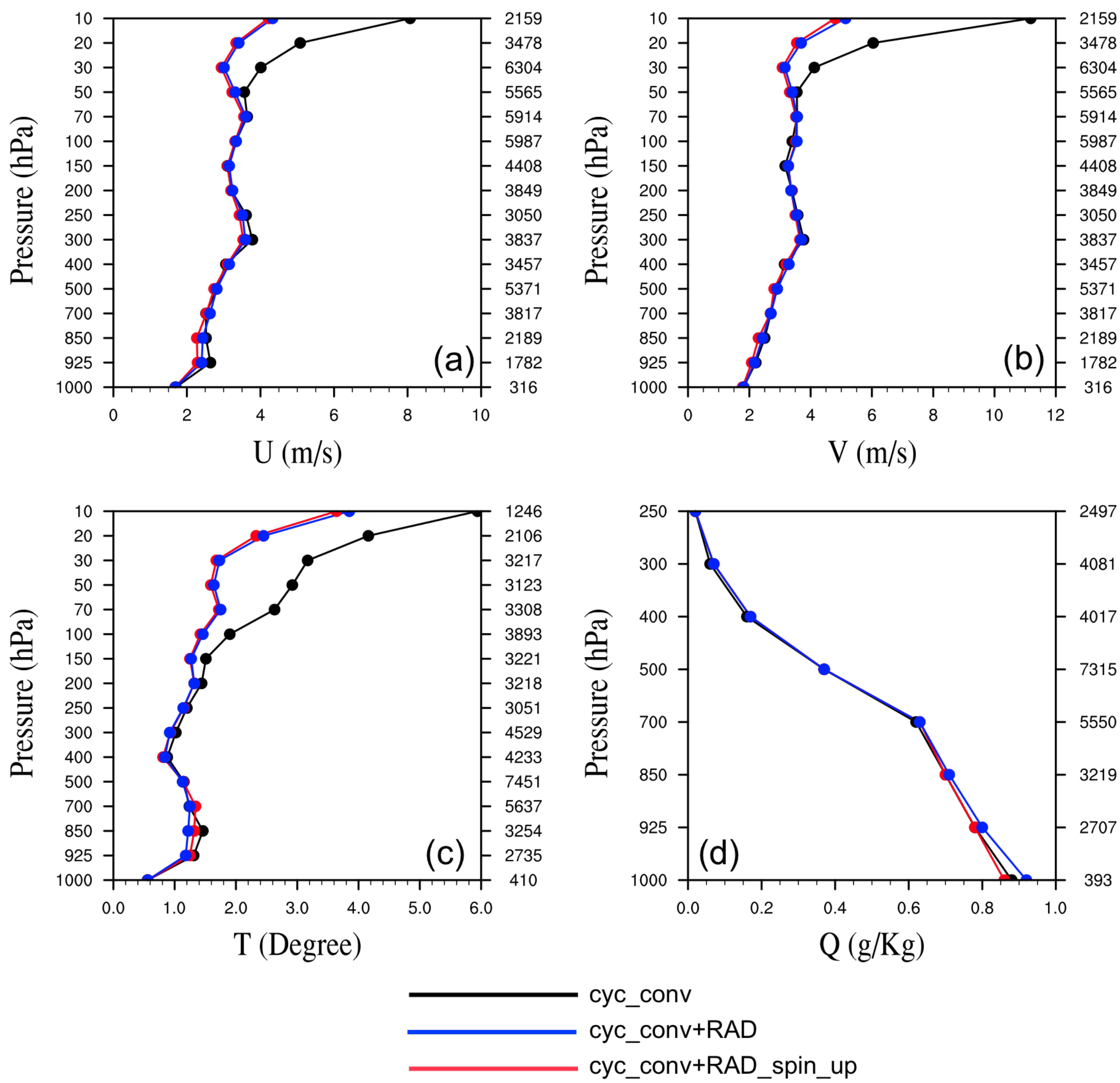

Fig. 18. RMSE aggregated over all initializations computed at all radiosonde locations within the domain at the analysis time. Meteorological variables and their units are specified on the figures: U—zonal wind component; V—meridional wind component; T—temperature; Q—water vapor mixing ratio. Numbers on the right y-axis denote the sample size at each pressure level.

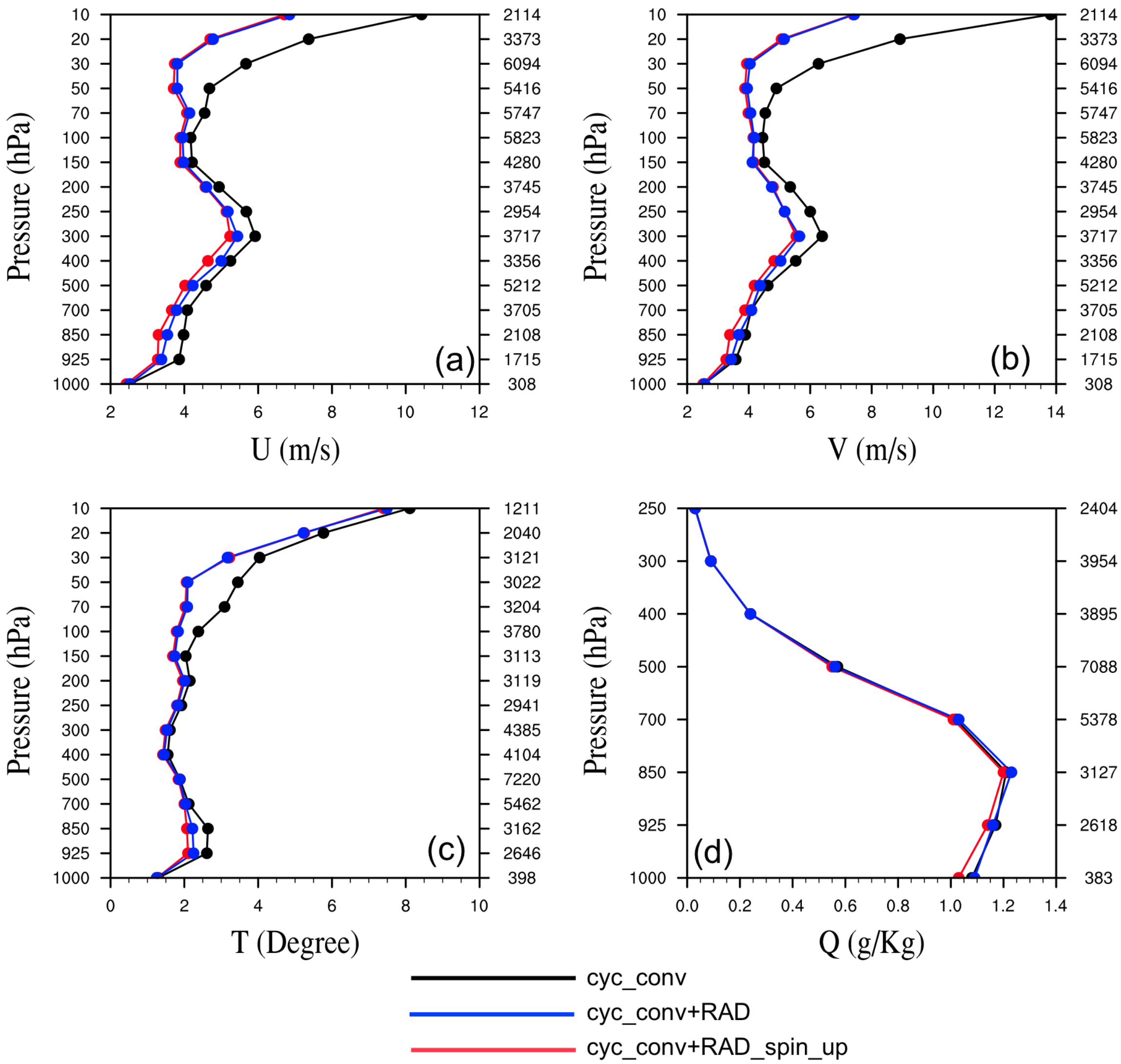

Fig. 19. As in Fig. 18 but for 24-hr forecasts.

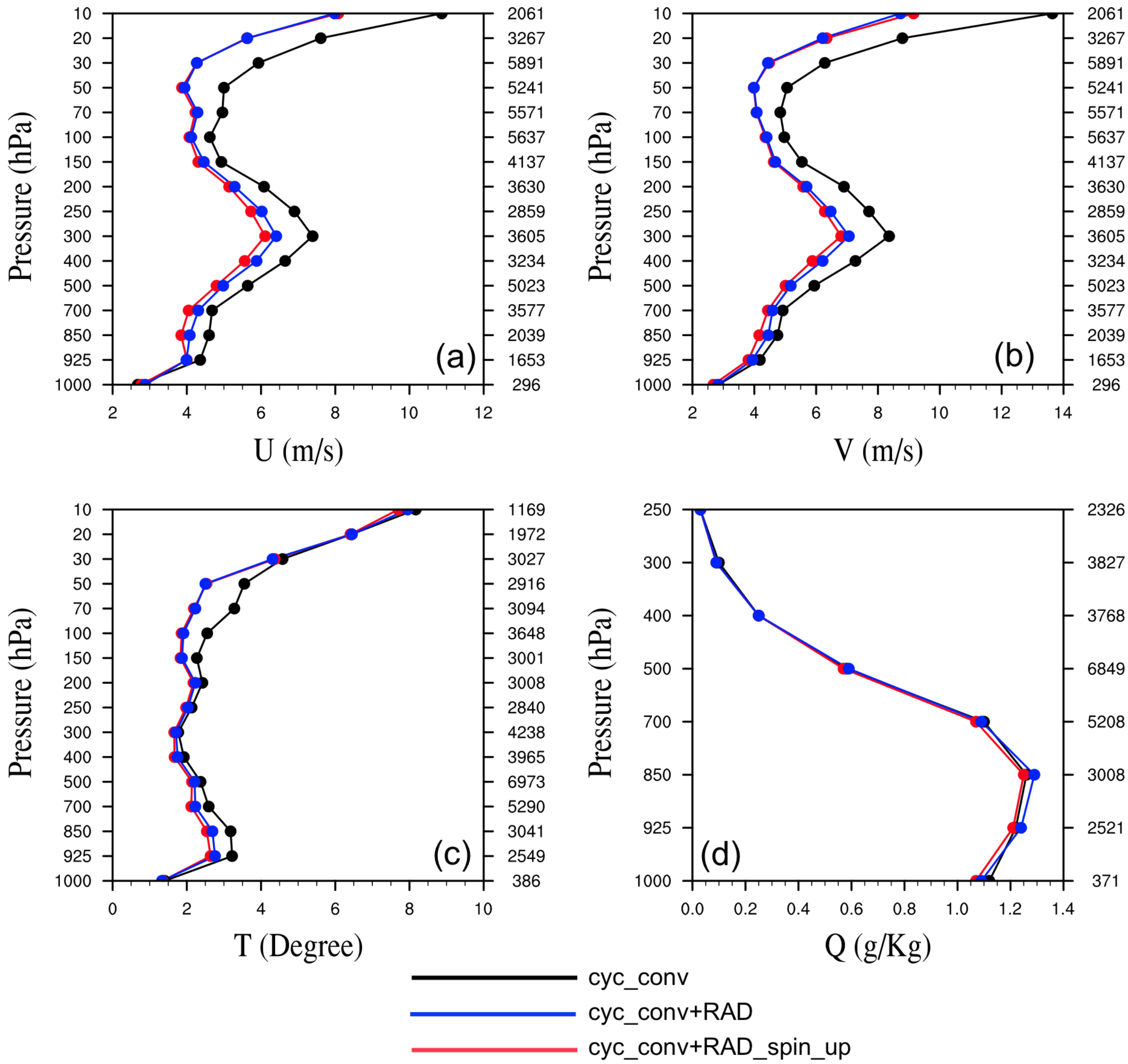

Fig. 20. As in Fig. 18 but for 48-hr forecasts.